The Journal of Neuroscience, July 1, 1996, *16*(13):4240–4249

Stimulus Specificity of Phase-Locked and Non-Phase-Locked 40 Hz Visual Responses in Human

Catherine Tallon-Baudry, Olivier Bertrand, Claude Delpuech, and Jacques Pernier

Brain Signals and Processing Laboratory, Institut National de la Santé et de la Recherche Médicale, F-69424 Lyon Cedex 03, France

Considerable interest has been raised by non-phase-locked episodes of synchronization in the gamma-band (30–60 Hz). One of their putative roles in the visual modality is feature-binding. We tested the stimulus specificity of high-frequency oscillations in humans using three types of visual stimuli: two coherent stimuli (a Kanizsa and a real triangle) and a noncoherent stimulus ("no-triangle stimulus"). The task of the subject was to count the occurrences of a curved illusory triangle. A time–frequency analysis of single-trial EEG data recorded from eight human subjects was performed to characterize phase-locked as well as non-phase-locked high-frequency activities.

We found an early phase-locked 40 Hz component, maximal at electrodes Cz–C4, which does not vary with stimulation type. We describe a second 40 Hz component, appearing around 280 msec, that is not phase-locked to stimulus onset. This component is stronger in response to a coherent triangle, whether real or illusory: it could reflect, therefore, a mechanism of feature binding based on high-frequency synchronization. Because both the illusory and the real triangle are more target-like, it could also correspond to an oscillatory mechanism for testing the match between stimulus and target. At the same latencies, the low-frequency evoked response components phase-locked to stimulus onset behave differently, suggesting that low- and high-frequency activities have different functional roles.

Key words: vision; feature binding; synchronization; 40 Hz; oscillations; gamma-band; human; evoked potentials; EEG

Milner (1974) presented a model for visual shape recognition in which synchronization of cell responses characterized a neuronal assembly coding for an object. This model suggested a mechanism for feature binding: cells responding to features belonging to the same object would discharge in synchrony. More recently, Singer's and Eckhorn's groups have reported experimental evidence for the existence of high-frequency synchronization in the visual cortex of the anesthetized cat, and checked the stimulus specificity of these oscillatory phenomena (Eckhorn et al., 1988; Gray and Singer, 1989; Gray et al., 1989, 1990; Engel et al., 1991). High-frequency (30–90 Hz) oscillations have also been described in the visual cortex of the awake macaque monkey (Kreiter and Singer, 1992; Eckhorn et al., 1993; Frien et al., 1994). However, the role of high-frequency synchronization in feature binding remains controversial because other groups either did not find any oscillatory activity (Tovee and Rolls, 1992; Young et al., 1992) or had doubts about their putative functional roles (Ghose and Freeman, 1992).

In the visual modality, 30–40 Hz EEG activities in humans are known to be elicited either by periodic visual stimulation (so called steady-state response) (Regan, 1968) or by a brief steady illumination (Chatrian, 1960). More recently, we reported the existence of a very small, although significant, increase of the averaged evoked potential around 32 Hz in response to coherent triangles, either real or illusory (Tallon et al., 1995). This component could be related to the oscillatory events observed in cat and monkey, because it seems dependent on stimulus coherency. Nevertheless, oscillatory events in cat and monkey have been shown to be non-phase-locked to stimulus onset (Eckhorn et al., 1988; Gray and Singer, 1989; Gray et al., 1989, 1990, 1992; Eckhorn et al., 1993; Brosch et al., 1995): therefore, they tend to disappear on averaged data. If the oscillatory activity we observed in the averaged evoked potential is indeed related to the local, intracortically recorded oscillatory events in animal, the small 40 Hz component we observed on the human scalp should correspond to a strong, but non-phase-locked, 40 Hz activity, partially canceled out by the averaging process.

Here, we analyze single-trial EEG data to characterize non-phase-locked activities in the time–frequency domain. We test the stimulus specificity of high-frequency activity with three stimuli: an illusory and a real triangle (coherent stimuli requiring some feature binding to be perceived, but also target-like), and a "no-triangle stimulus" (noncoherent one, and not target-like). The task of the subject was to count the occurrences of a curved illusory triangle (Fig. 1).

MATERIALS AND METHODS

Subjects. Eight right-handed subjects were recorded (4 males, 4 females, mean age 23 years). All subjects had normal or corrected-to-normal vision and could easily perceive illusory contours. The study was performed with the written consent of each subject.

Stimuli. Three types of stimuli were delivered (Fig. 1): an illusory triangle (Kanizsa, 1976), a real triangle, and a control stimulus we will refer to as a "no-triangle stimulus." This no-triangle stimulus was built by rotating the inducer disks of the illusory triangle so that the illusion disappears. The subjects' task was to count silently an additional target distractor, a curved illusory triangle. This target was delivered randomly, intermixed with the three stimuli. This task ensured that subjects correctly perceived illusory contours and remained attentive throughout the entire recording session. Subjects were trained to perform this task for few minutes before the beginning of the experiment. The target stimulus will not be included in the analysis, because we would not be able to disen-

Received Jan. 31, 1996; revised April 10, 1996; accepted April 16, 1996.

We thank J. F. Echallier for helpful technical assistance.

Correspondence should be addressed to Catherine Tallon-Baudry, Brain Signals and Processing Laboratory, INSERM U280, 151 cours Albert Thomas, F-69424 Lyon Cedex 03, France.

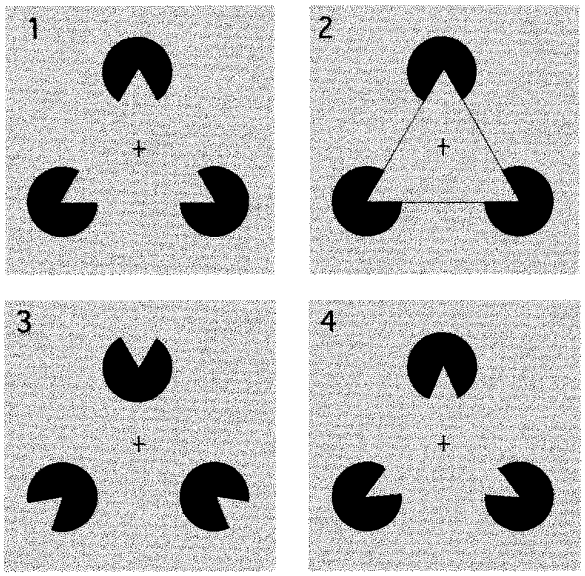

Figure 1. Stimuli. We used three types of nontarget stimuli: an illusory triangle (Kanizsa triangle) (*1*), a real triangle (*2*), and what we called a "no-triangle stimulus" (*3*). Subjects were instructed to count silently the occurrences of an additional target distractor, a curved illusory triangle (*4*). This task, when correctly performed, ensured that subjects perceived illusory contours.

tangle target detection and counting mechanisms from perception mechanisms.

Stimuli were equiprobably delivered on a video display for 700 msec in a randomized order. Interstimulus interval was randomized between 2 and 3 sec. Stimuli subtended a visual angle of 2.5° at a viewing distance of 2 m, and they were displayed on a light gray background. The ratio between the diameter of the inducing disk and the total length of the edge of the triangle was 1:4. The fixation point was a small, dark brown cross permanently displayed on the center of the screen.

Recordings. EEG was continuously recorded at a sampling rate of 1000 Hz (0.1–320 Hz analog bandwidth) from 13 Ag/AgCl electrodes referenced to the nose. Their locations according to the international 10–20 system were: Iz, T5, O1, O2, T6, POz, P3, Pz, P4, C3, Cz, C4, and Fz. Electrode placement on the head was assisted by a computer-based system (Echallier et al., 1992). Electrode impedances were kept below 5 kΩ. Horizontal and vertical eye movements were monitored, and a rejection threshold was set for each subject at the potential value corresponding to a saccade to one of the vertices of the triangle. Eight blocks of 90 stimuli were delivered to each subject. Epochs containing artifacts (EEG $>$ 100 μV or EOG $>$ threshold), from 350 msec before to 800 msec after stimulus onset, were rejected off-line. Sixty-six percent of the responses were considered artifact-free, corresponding to a mean of 154 artifact-free responses per subject and per stimulation type.

Data analysis. We are interested in the identification and characterization of oscillatory activities induced by a stimulation. Because both latency and frequency of these oscillatory bursts are not known a priori, a method that preserves both types of information was chosen: the time–frequency representation based on wavelet transform of the signals. In previous reports of human gamma-band analysis, a method has been proposed to estimate the event-related spectral perturbation (Makeig, 1993) using short-term Fourier transforms computed on the EEG tapered by a moving Hanning window of constant duration. The window duration, therefore, is the same for all frequency bands. Instead, we used an estimation of the time–frequency energy based on the wavelet transform of the signal: because the duration of the window is shorter for higher-frequency bands, it provides a better compromise between time and frequency resolutions (Sinkkonen et al., 1995). This analysis, applied to the average evoked potential, mainly provides information on phase-locked oscillatory bursts. When applied to single trials, it allows identification of non-phase-locked activities, as long as their signal-to-noise ratio is high enough. A "phase-averaging" technique is proposed to quantify phase-locking of oscillatory bursts, irrespective of their amplitude.

The signal was convoluted by complex Morlet's wavelets $w(t, f_0)$ (Kronland-Martinet et al., 1987) having a Gaussian shape both in the time domain (SD σ_t) and in the frequency domain (SD σ_f) around its central frequency f_0: $w(t, f_0) = A \cdot \exp(-t^2/2\sigma_t^2) \cdot \exp(2i\pi f_0 t)$, with $\sigma_f = 1/2\pi\sigma_t$. Wavelets were normalized so that their total energy was 1, the normalization factor A being equal to $(\sigma_t\sqrt{\pi})^{-1/2}$. A wavelet family is characterized by a constant ratio (f_0/σ_f), which should be chosen in practice greater than ~5 (Grosmann et al., 1989). The wavelet family we used was defined by $f_0/\sigma_f = 7$, with f_0 ranging from 20 to 100 Hz in 1 Hz step. At 20 Hz, this leads to a wavelet duration $(2\sigma_t)$ of 111.4 msec and to a spectral bandwidth $(2\sigma_f)$ of 5.8 Hz and, at 100 Hz, to a duration of 22.2 msec and a bandwidth of 28.6 Hz. The time resolution of this method, therefore, increases with frequency, whereas the frequency resolution decreases. Below 20 Hz, wavelet duration is of hundreds of milliseconds: non-phase-locked low-frequency components thus require very long epochs of EEG to be correctly analyzed. Because our study aims specifically analyzing a possible functional role of the stimulus-related gamma-band oscillatory activity, the time–frequency analysis of phase-locked and non-phase-locked components will be focused on the 20–100 Hz frequency range. Nevertheless, we will compare with a similar temporal resolution our results to the standard averaged evoked response (low-frequency phase-locked activity only).

The time-varying energy $E(t, f_0)$ of the signal in a frequency band around f_0 is the squared norm of the result of the convolution of a complex wavelet $w(t, f_0)$ with the signal $s(t)$: $E(t, f_0) = w(t, f_0) \cdot s(t)^2$. A family of wavelets will provide a time–frequency representation of the energy of the signal (TF energy). This approach can be applied to the averaged evoked potential or to each single trial. The TF energy of the averaged evoked potential allows us to characterize phase-locked activities, while by averaging the TF energy of each single trial, both phase-locked and non-phase-locked activities are summed. In the latter case, noise energy is also added up: only high signal-to-noise-ratio activities will emerge. The mean TF energy of the prestimulus (between −200 and −50 msec) is considered a baseline level and is subtracted from the pre- and poststimulus TF energy. This correction is done separately in each frequency band.

The phase-locking of the oscillatory burst can be evaluated in the time–frequency domain by adapting the "phase-averaging" methods previously proposed in the frequency domain by Jervis et al. (1983). We consider the normalized complex time-varying energy of each single trial i: $P_i(t, f_0) = w(t, f_0) \cdot s_i(t)/|w(t, f_0) \cdot s_i(t)|$. Averaging these quantities across single trials leads to a complex value related to the phase distribution of each time–frequency region around t and f_0. The modulus of this value will be called the "phase-locking factor." It ranges from 0 (purely non-phase-locked activity) to 1 (strictly phase-locked activity). With this method, even very low-amplitude signals can be identified provided they are rather strictly phase-locked. Furthermore, it has been shown to be robust against artifacts. To detect phase ordering, a statistical test (Rayleigh test) of uniformity of angle is used (Jervis et al., 1983).

Because our data are far from having a normal distribution, the nonparametric Quade test for related samples and Conover procedures as post hoc tests of significance were used (Conover, 1980). This test is an extension of the Wilcoxon signed-ranks test to the case of several related samples. It is performed by ranking data paired by subjects and provides an F value indicating whether there is a statistically significant global effect of stimulation type. If the effect is significant, Conover procedures can determine in which pairs of experimental conditions significant differences occur. To reduce the effect of intersubject variability in frequency and latency, this test was applied to mean TF energy values within a 100 msec × 15 Hz window. This window was regularly shifted by 16 msec in time and 3 Hz in frequency to cover the entire time–frequency plane.

RESULTS

Identification of three components in the time–frequency domain

We first averaged the TF energy across single trials to analyze both phase-locked and non-phase-locked activities. Two successive components of the gamma-band (30–60 Hz) response can be seen at electrode Cz (Fig. 2, *top row*): one at ~90 msec, 40 Hz, and another one near 280 msec, extending from 30 Hz up to ~70 Hz. Between these two peaks, the level of 30–80 Hz energy is lower than in the prestimulus period.

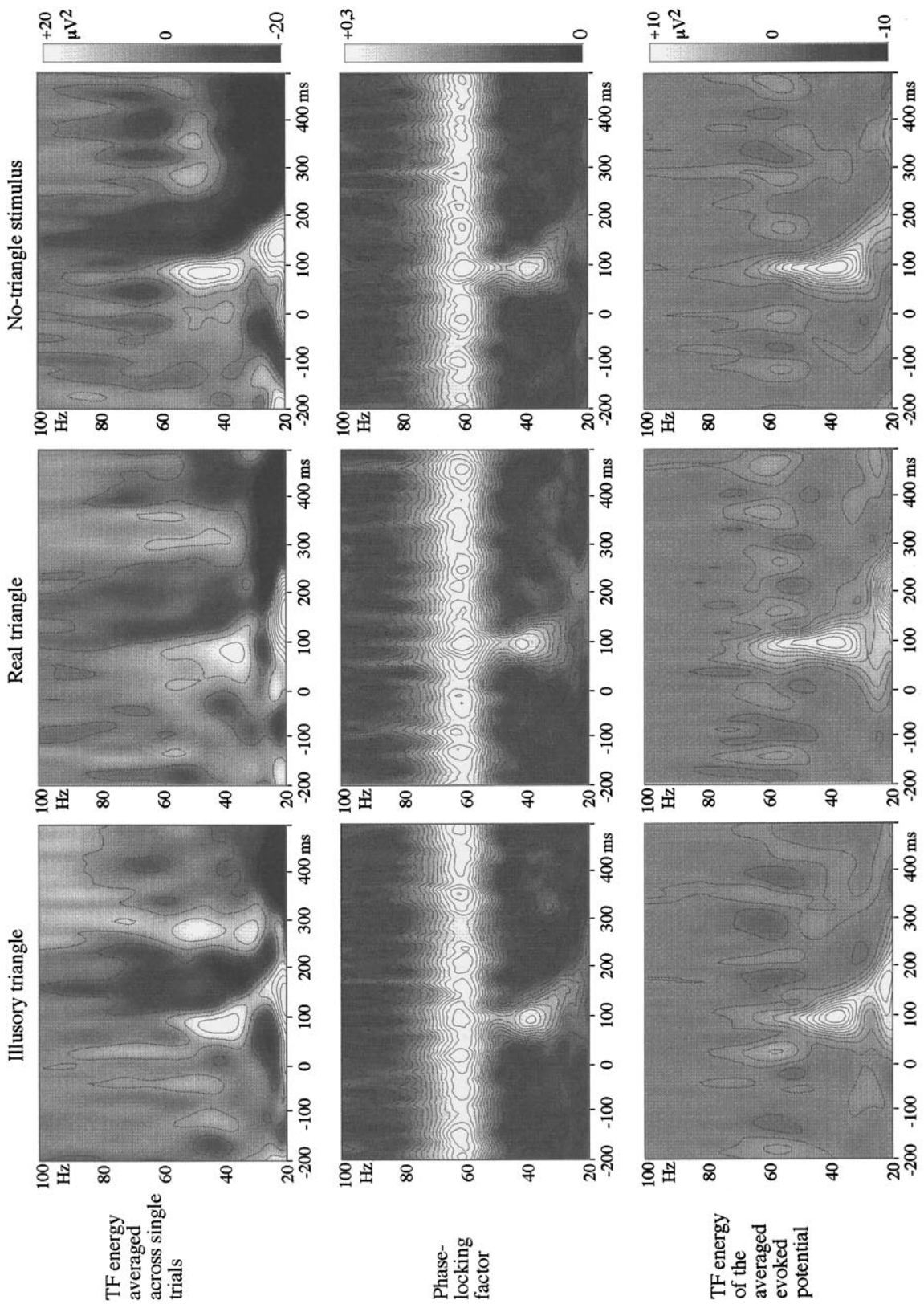

Figure 2. Time–frequency analysis at electrode Cz, grand average across subjects. *Top row*, TF energy averaged across single trials. This type of averaging sums phase-locked as well as non-phase-locked activities. Results are baseline-corrected (subtraction of the prestimulus levels in each frequency band), thus producing positive and negative values. Two successive increases of TF energy can be observed: a first one around 90 msec and a second one around 280 msec. *Middle row,* Phase-locking factor. The first gamma-band component (90 msec) is phase-locked to stimulus onset, whereas the second one (280 msec) disappears: it is not phase-locked. Data are not baseline-corrected: the artifact created by our video monitor, therefore, is prominent (continuous component at 62 Hz, video frame rate). *Bottom row,* Baseline-corrected TF energy of the averaged evoked potential. Only phase-locked components of the response can be seen, but with a better signal-to-noise ratio. There are no TF energy differences between stimulation types for the 40 Hz, 90 msec component.

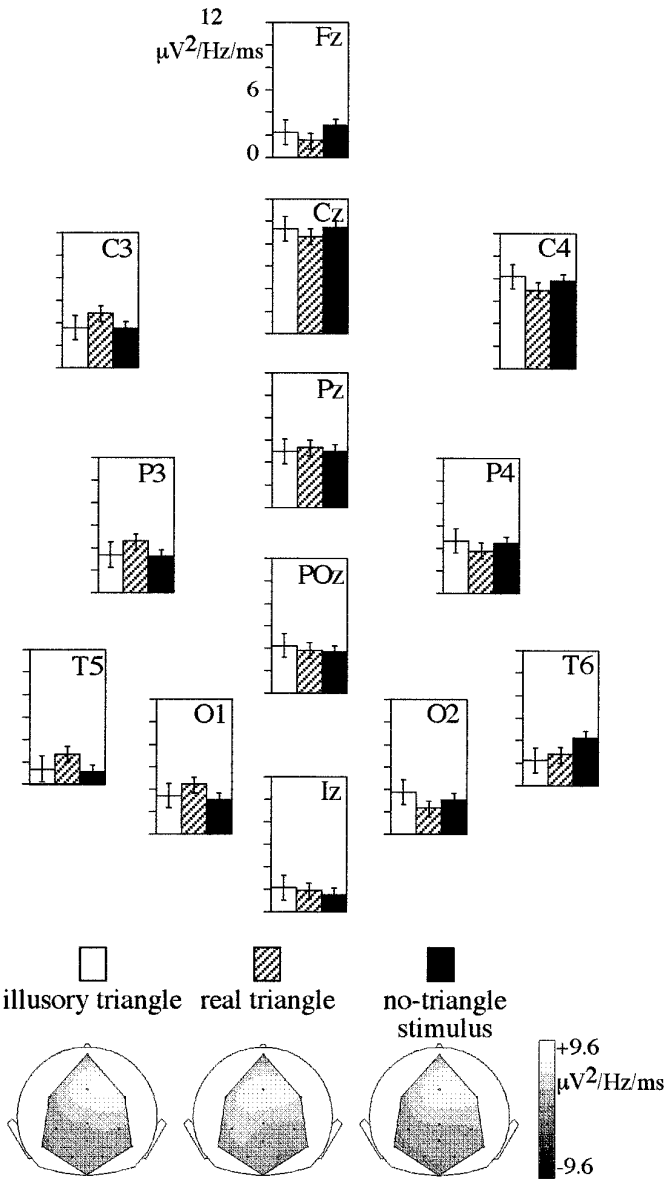

Figure 3. Energy of the first component, considered as the mean value between 70 and 120 msec and 30 and 50 Hz of the TF energy of the averaged evoked potential. The topography of this component is rather focal, with a clear maximum at electrodes *Cz–C4*. No variation with stimulation type can be observed.

Both the 100 msec, 40 Hz and the 280 msec, 30–70 Hz components seem to be distinct from the lower frequency components of the response, because the TF energy decreases at ~25 Hz and increases again at higher frequencies. We will thus call "low frequencies" frequencies ranging from 0 to 25 Hz, and "high frequencies" those ranging from 25 to 100 Hz. Because the time–frequency analysis we developed gives a poor time resolution for frequencies below 15 Hz, low-frequency components will be studied in the 0–25 Hz filtered averaged evoked potential, whereas time–frequency representations will be used for high-frequency components.

The second step in our analysis was "phase averaging": it allows characterization of phase-locked activities regardless of their amplitude. Results at electrode Cz are shown in Figure 2 (*middle row*).

Table 1. Energy, latency, and frequency of the maximum of the first 40 Hz response, measured on the TF energy of the averaged evoked potential

	Energy (μV^2)			Latency (msec)			Frequency (Hz)		
	Illusory	Real	No	Illusory	Real	No	Illusory	Real	No
Mean	19.5	21.9	19.9	99	89	89.5	37.9	42.2	38.5
SEM	5.4	4.8	3.8	6.2	6.4	2.6	3.2	3.2	2.7

No significant differences can be found among conditions.

The 90 msec, 40 Hz component appears to be phase-locked to stimulus onset. Indeed, all subjects show a significantly phase-locked component around 90 msec and 40 Hz (Rayleigh test at electrode Cz: $p < 0.001$ for 7 of 8 subjects, $p < 0.01$ for all subjects). This part of the response will be studied, therefore, in the time–frequency representation of the energy of the averaged evoked potential, to be in a better signal-to-noise ratio situation (Fig. 2, *bottom row*).

The second gamma-range component disappears completely on the time–frequency representation of the phase-locking factor. This component, therefore, is not strictly phase-locked to stimulus onset and will be studied on the TF energy averaged across single trials.

A continuous phase-locked activity centered at 62 Hz appearing on the time–frequency representation of the phase-locking factor corresponds to the frame rate of the video monitor on which stimuli were delivered. This activity is continuous (same level on the pre- and poststimulus TF representation of the phase-locking factor), and thus disappears on baseline-subtracted representations of TF energy (Fig. 2, *top* and *bottom rows*).

We thus found two different types of high-frequency activities: an early one (90 msec) phase-locked to stimulus onset, and another one appearing later (280 msec), not phase-locked to stimulus onset. Both responses seem to be distinct from low-frequency potentials (0–25 Hz). These results are similar at all electrodes.

These findings led us to divide the entire electrical response into three components, each one analyzed using the appropriate method:

(1) low-frequency phase-locked components (0–25 Hz): analysis of the low-pass-filtered averaged evoked potential.
(2) phase-locked, high-frequency early components (20–100 Hz, 0–200 msec): analysis of the TF energy of the averaged evoked potential.
(3) non-phase-locked, high-frequency late components (20–100 Hz, 200–500 msec): analysis of the TF energy averaged across single trials.

First burst (TF energy of the averaged evoked potential)

The first burst of 40 Hz activity is phase-locked to the stimulus onset and thus appears with a better signal-to-noise ratio on the time–frequency representation of the energy of the averaged evoked potential (Fig. 2, *bottom row*).

This first 40 Hz component shows a clear maximum at electrodes Cz and C4, as depicted in Figure 3. There does not seem to be any difference between experimental conditions at these electrodes. To confirm this, we first searched for the maximal TF energy across electrodes, for each subject and each stimulus condition. This maximum always occurred at electrode Cz or C4, except for one subject whose maximum appeared at P4. We

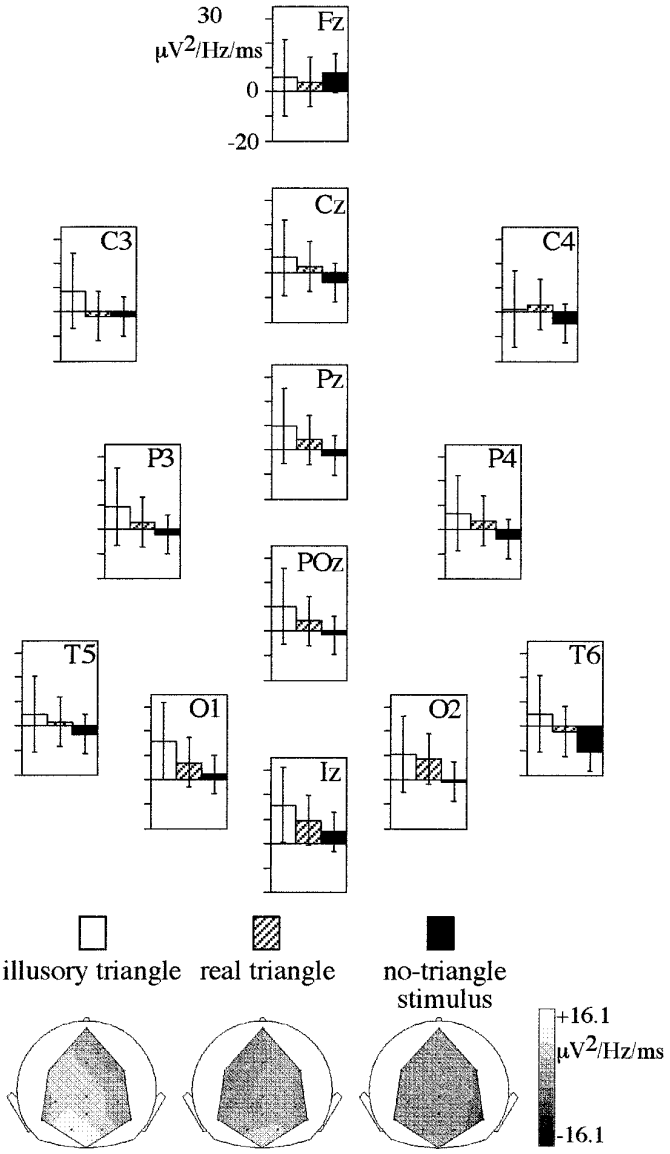

Figure 4. Energy of the second component, considered as the mean value between 250 and 350 msec and 30 and 70 Hz of the TF energy averaged across single trials. The topography of this component is widespread, with a weak maximum at occipital electrodes (*O1*, *Iz*, *O2*). There seems to be a maximum of energy in response to the illusory triangle, an intermediate value in response to the real triangle, and a small one in response to the no-triangle stimulus.

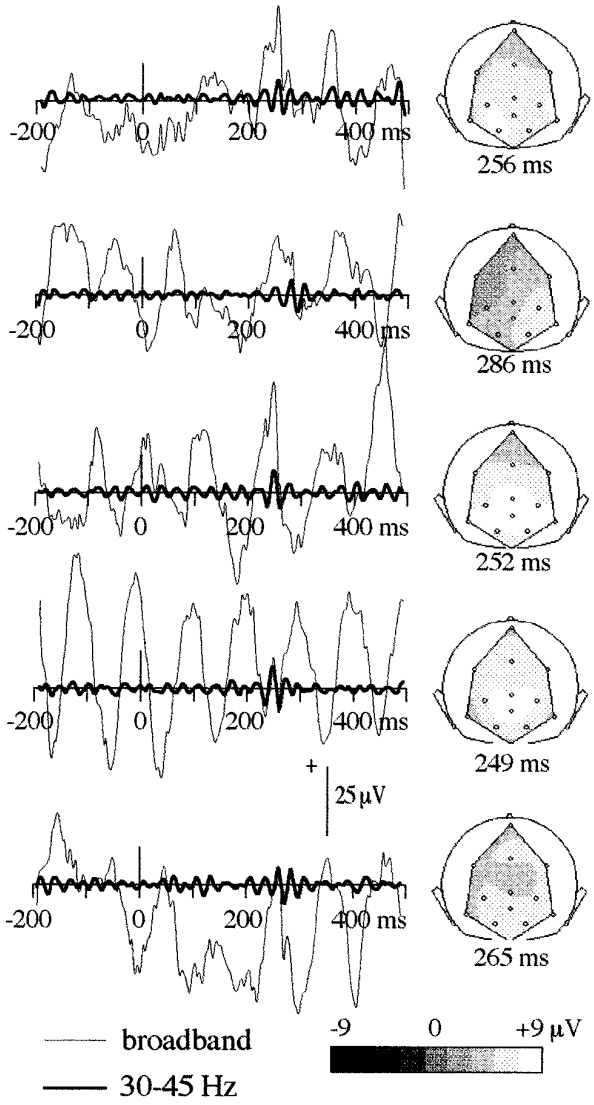

Figure 5. 30–45 Hz filtered (*thick lines*) and broad-band (*thin lines*) single trials at electrode POz and topography of each 30–45 Hz filtered response at the latency of the maximal positive peak. Oscillatory episodes are rather brief (from 100 to 150 msec) and of high amplitude (up to 10 μV), even though the amplitude of the broad-band response is higher. They are not phase-locked to stimulus onset (indicated by the *vertical bar* at 0 msec). Their topography is widespread, without any polarity inversion; a maximum is usually located at occipital or parietal electrodes.

measured its TF energy, latency, and frequency. Results are summarized in Table 1: the maximal TF energy does not vary with stimulation type. It tends to appear later in the illusory triangle condition, and at a higher frequency in the real triangle condition, but neither of these two observations is significant (Wilcoxon test for matched pairs, $p > 0.1$).

We then performed a Quade test on the time–frequency representation of the energy of the averaged evoked potential, at electrodes Cz and C4, in smoothing windows of 100 msec × 15 Hz, shifted by steps of 16 msec in time and of 3 Hz in frequency (between 0 and 200 msec, and between 20 and 100 Hz). This analysis confirmed that there were no significant differences between stimulation types.

Second burst (TF energy averaged across single trials)

The topography of the second burst is less clear than the topography of the first burst: on data averaged across subjects (Fig. 4), no clear maximum can be found, even though the TF energy at posterior electrodes seems slightly higher than at anterior ones. We searched for the location of the maximal TF energy between 250 and 350 msec, and between 30 and 70 Hz, for each subject and in each condition. In seven of eight subjects, this maximum is reached at electrodes posterior to Pz in all experimental conditions.

Visual inspection of filtered single trials on which a 30–45 Hz component could be identified confirms this widespread topography, as well as the posterior location of the maximum (Fig. 5). No polarity inversion can be observed. Furthermore, it appears that (1) the oscillatory events are rather short (from 100 to 150 msec),

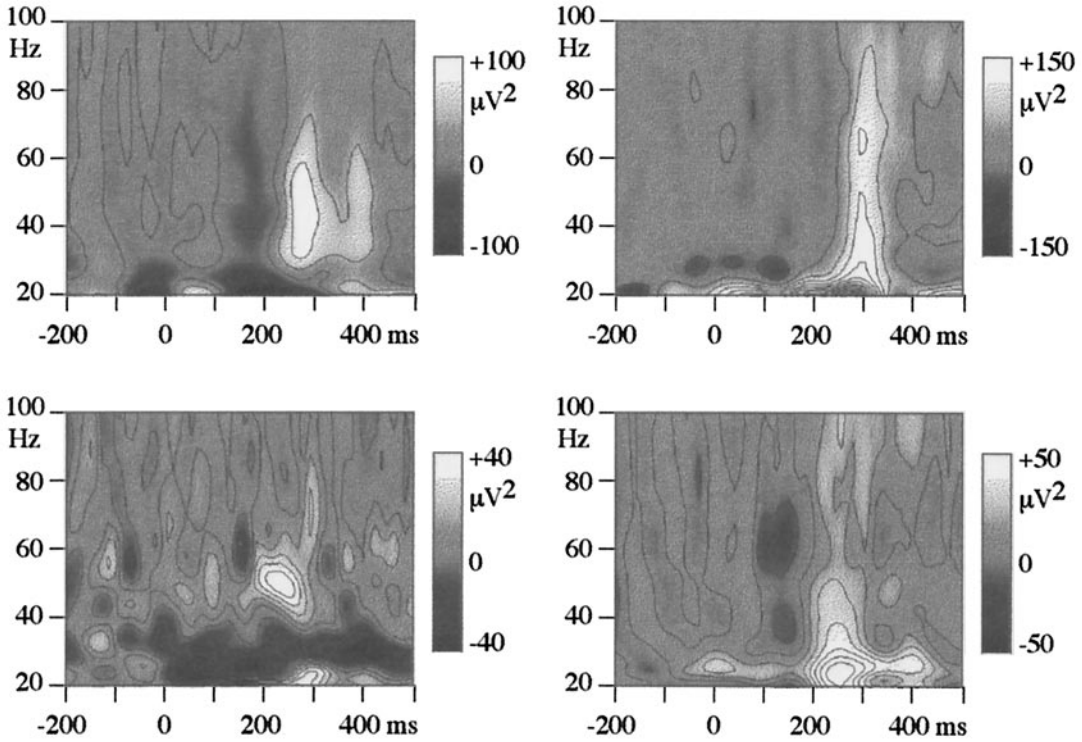

Figure 6. TF energy averaged across single trials of four different subjects, at electrode POz, in response to the illusory triangle. Note the strong intersubject variability of the non-phase-locked, 280 msec component (energy of the maximum ranging from 40 to 150 μV^2 and frequency from 25 to 65 Hz).

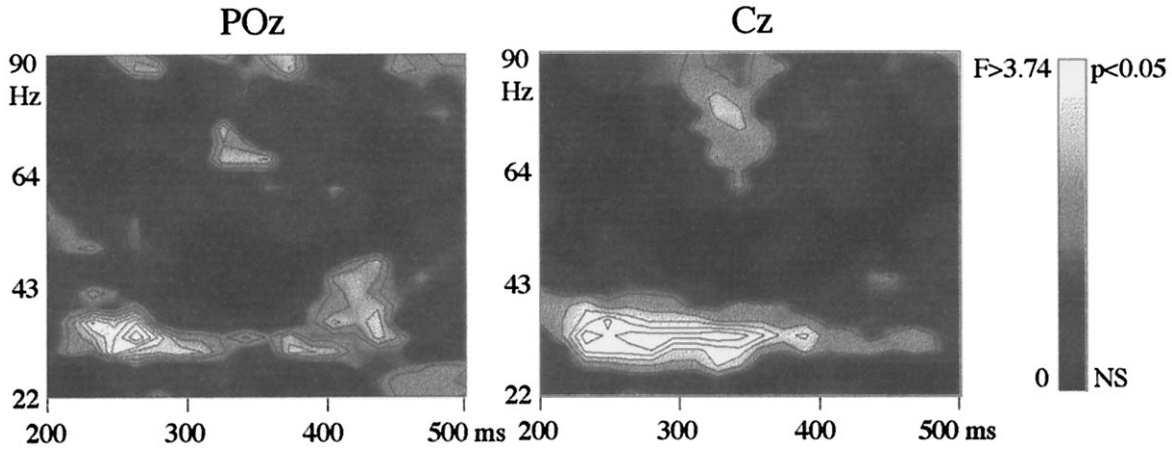

Figure 7. Quade test: *F*-values at electrodes *POz* and *Cz*. A Quade test was performed on the energy averaged across single trials, on 100 msec × 15 Hz moving time–frequency windows. $F > 3.74$ (in *white*) at *x* msec and *y* Hz indicates a significant effect ($p < 0.05$) of the stimulation type in the 100 msec × 15 Hz time–frequency window centered in (*x*,*y*). The duration of the significant effect may vary from electrode to electrode, but the effect is always confined to the 30–40 Hz range.

(2) their amplitude can reach up to 10 μV, and (3) the latency of the maximal positive peak can vary by at least as much as 37 msec.

The intersubject variability of this second burst is quite strong, in energy as well as in frequency, as depicted in Figure 6.

TF energy variations with stimulation type seem distributed over all of the electrodes, with a high response to the illusory triangle, an intermediate response to the real triangle, and a weak (or even sometimes below baseline) response to the no-triangle stimulus (Fig. 4).

We performed a Quade test on the time–frequency representation of the energy averaged across single trials, at each electrode, in smoothing windows of 100 msec × 15 Hz, shifted by steps of 16 msec in time and of 3 Hz in frequency (between 200 and 500 msec and 20 and 100 Hz). At all electrodes but Iz, O2, T6, and Fz, the test shows a significant effect of the stimulation type in a window centered at 250 msec and 35 Hz. The size of this window (mainly its time–length) varies with electrodes (Fig. 7). The effect is confined to the 30–40 Hz range: no effect can be found at higher frequencies.

Within this region (around 250 msec and 35 Hz) where a significant stimulus effect is found, the Conover procedures show two types of effects: either the response to the illusory triangle is significantly

Table 2. Maximal time–frequency window on which a significant effect can be found (Quade test, $p < 0.05$), measured on the TF energy averaged across single trials

	Illusory and real > no-triangle		Illusory > no-triangle	
T5	25–42 Hz	200–280 msec	none	
O1	none		30–45 Hz	200–280 msec
POz	30–45 Hz	210–270 msec	28–45 Hz	200–300 msec
P3	28–38 Hz	200–300 msec	25–42 Hz	200–290 msec
Pz	30–42 Hz	210–290 msec	25–45 Hz	200–400 msec
P4	30–40 Hz	210–280 msec	30–40 Hz	200–400 msec
Cz	28–45 Hz	200–300 msec	25–50 Hz	200–400 msec
C4	none		28–38 Hz	200–300 msec

stronger than the response to the no-triangle stimulus, or both the responses to the illusory and the real triangles are significantly higher than the response to the no-triangle stimulus (Quade test and Conover procedures, $p < 0.05$). The energies of the real and of the illusory triangles are never significantly different.

At each electrode at which an effect of the stimulation type could be found, we searched for the largest time–frequency window in which both the responses to the illusory and the real triangle were significantly higher than the response to the no-triangle stimulus, and for the largest time–frequency window in which the response to the illusory triangle was significantly higher than the response to the no-triangle stimulus. Results are shown on Table 2. It appears that in a 200–300 msec, 30–40 Hz window, both the real and the illusory triangles give rise to a stronger response than the no-triangle stimulus, and that between 300 and 400 msec, and 30 and 40 Hz, only the difference between the illusory and the no-triangle stimulus remains significant. Within this region, the TF energy of the response to the real triangle is intermediate between the two others.

Low-frequency averaged evoked potentials (filtered 0–25 Hz)

The usual complex of a first positive peak (P1) followed by a negative one (N1) can be observed in the averaged evoked potentials in response to the three stimuli. These two components are maximal at occipital electrodes (P1: O1, O2, or POz; N1: T5, O1, O2, or T6, depending on the subjects). We measured the P1 and N1 maximal amplitude values and their peak latencies, for each subject in each condition (Table 3). No differences among stimulus types could be found.

Later on, two successive effects can be found in the evoked potentials, as depicted in Figure 8 (Quade test and Conover procedures applied on 100 msec time windows regularly shifted by 20 msec, $p < 0.05$). The first appears between 200 and 300 msec and corresponds to a more negative potential in response to the illusory triangle than to the two other stimuli. This effect can be found at all electrodes, but appears earlier at occipital electrodes. The second effect appears between 300 and 400 msec, and corresponds to higher values of potential for the real triangle than the two others. It affects a more limited set of electrodes, on the right side of the head (Fig. 8). Both effects are mainly attributable to the very low-frequency components of the evoked potential (<8 Hz); they are no longer significant in the 8–25 Hz filtered evoked potentials.

DISCUSSION

We thus found the following:

• around 90 msec a 40 Hz component, phase-locked to the stimulus onset, appears. This component is maximal at electrodes Cz and C4. At the same time, the first positive peak (P1) of the low-frequency evoked potential is rising. It reaches its maximum at 113 msec at occipital electrodes (O1, O2 or POz, depending on the subjects). The different topographies of the low- and high-frequency phase-locked components are shown in Figure 9. Neither these two components vary with stimulus type.

• between 200 and 300 msec, a non-phase-locked, 30–40 Hz component appears. It is significantly stronger in response to both real and illusory triangles. At the same time, a very low-frequency component (0–8 Hz) appears in the evoked response. This component is more negative in response to the illusory triangle than to the real or the no triangle. Both these low- and high-frequency effects are rather spread out on the scalp and are significant at most electrodes.

• between 300 and 400 msec, the non-phase-locked, 30–40 Hz component is significantly stronger in response to the illusory triangle than in response to the no-triangle. The 40 Hz response to the real triangle is intermediate between the two others. At the same latencies, low-frequency evoked potentials are more positive in response to the real triangle compared with the illusory or the no-triangle stimulus.

Table 3. Latency and amplitude of the P1 and N1 of the averaged evoked potential (0–25 Hz): mean ± SEM

	P1		N1	
	Latency (msec)	Maximum (μV)	Latency (msec)	Maximum (μV)
Illusory triangle	113.1 ± 3.8	11.9 ± 2.0	166.2 ± 3.1	−19.64 ± 1.9
Real triangle	112.00 ± 4.0	10.6 ± 1.7	162.7 ± 3.9	−18.59 ± 2.0
No triangle	114.9 ± 5.4	12.0 ± 1.6	165.2 ± 3.6	−17.96 ± 1.5

The functional role of the first 40 Hz, phase-locked component remains unclear. An early 40 Hz component appearing in averaged evoked potentials has been described by Jokeit et al. (1994) in response to a visual stimulus in a priming reaction time task. It may be that this component appears in response to any visual stimulus in any task. This 40 Hz component could also be part of a broad-band activity including the P1 low-frequency component, because neither of these two components varies with stimulation type. Still, their topographies and latencies are different, suggesting that they reflect the activity of different neural sources.

In the auditory modality, an early, transient 40 Hz response can be observed in the averaged evoked potential (Galambos et al., 1981; Pantev et al., 1991) and has been suggested to reflect the activation of thalamo-cortical loops (Ribary et al., 1991; Llinás and Ribary, 1993). Both the early 40 Hz response and the low-frequency potentials have similar topographies (Bertrand and Pantev, 1994), whereas in the visual modality, they are quite different. We do not know yet whether there is a functional analogy between the two modalities.

Short-latency, stimulus-locked, high-frequency responses in V1 of the behaving macaque monkey have been described (Maunsell and Gibson, 1992). There is quite a difference in the latency of the two phenomenon (before 50 msec in monkey, and around 90 msec in human) and in their frequency (50–100 Hz in monkey, 40 Hz in human). Furthermore, an activity restricted to area V1 is not likely to appear on the scalp with a maximum at electrodes Cz and C4. It is still possible that the phase-locked activity we observe on the scalp reflects a combination of activation in V1 and other areas.

The non-phase-locked 40 Hz component occurring between 200 and 400 msec varies with stimulation type: it is stronger in re-

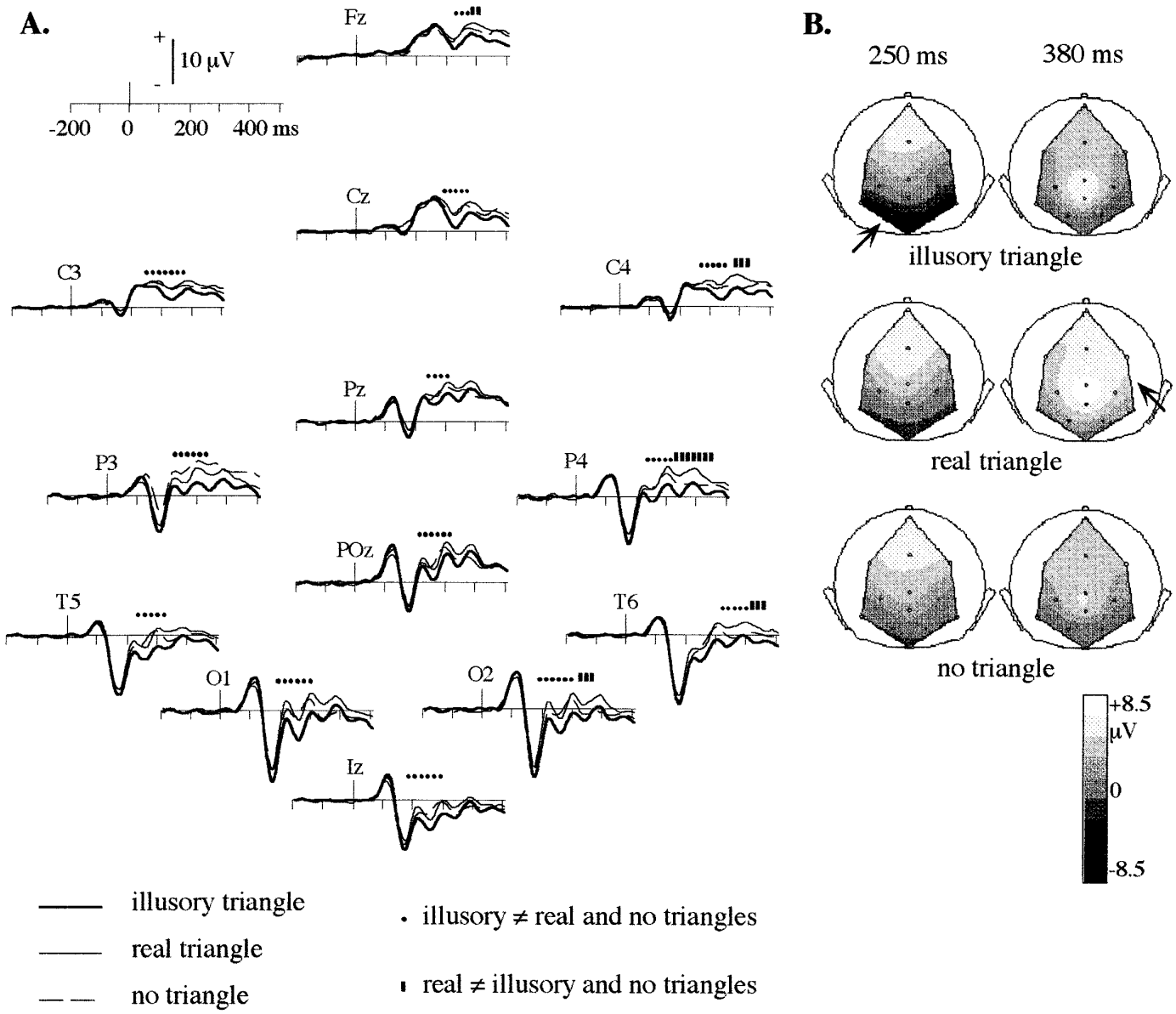

Figure 8. *A*, 0–25 Hz filtered averaged evoked potentials. We performed a Quade test and Conover procedures on the averaged evoked potential, computed over 100 msec time windows regularly shifted by 20 msec. Two successive effects can be found. They are plotted on the figure as *dots* or *bars* indicating the center of the 100 msec time window on which an effect has been found. A first effect occurs on all of the electrodes between 200 and 300 msec; it corresponds to potentials more negative for the illusory triangle than for the two others (*dots*). The second effect concerns a more limited set of electrodes and appears between 300 and 400 msec. It corresponds to a greater positivity in response to the real triangle than the two others (*bars*). *B*, Topography of the 0–25 Hz averaged evoked potential (grand average across subjects) at two latencies (250 and 380 msec) in each condition. At 250 msec, the response to the illusory triangle shows a more pronounced negativity at occipital and parietal electrodes. At 380 msec, the real triangle elicits a more positive response than the two others on the right side of the scalp.

sponse to a coherent triangle, whether real or illusory. At least two mechanisms can account for this: (1) an oscillatory mechanism of feature binding as suggested by Singer's and Eckhorn's groups (Engel et al., 1992; Eckhorn, 1994): neurons responding to the triangle (real or illusory) would discharge in synchrony around 35 Hz, or (2) an oscillatory matching mechanism between an internal representation of the target stimulus (curved triangle) and the occurring stimulus. Because both the illusory and the real triangles look more like the attended target, they may give rise to a stronger matching. A possible control would be a target stimulus looking more like the no-triangle stimulus. Nevertheless, the correct perception of illusory contours would not be ensured in such an experimental design. This raises the problem of the links among the processes of perception, recognition, and attention. Many different stimulus types and tasks will have to be used to determine whether the non-phase-locked 40 Hz component we observe in humans does reflect feature binding, visual matching, or another mechanism of perception.

It seems unlikely that this component could correspond to muscle activity, because the effect is confined between 30 and 40 Hz. If muscle activity were involved, one would expect to find at least some effects at higher frequencies (>60 Hz), and the topography of the activity would probably not show a maximum at parieto-occipital electrodes. It also seems unlikely that this com-

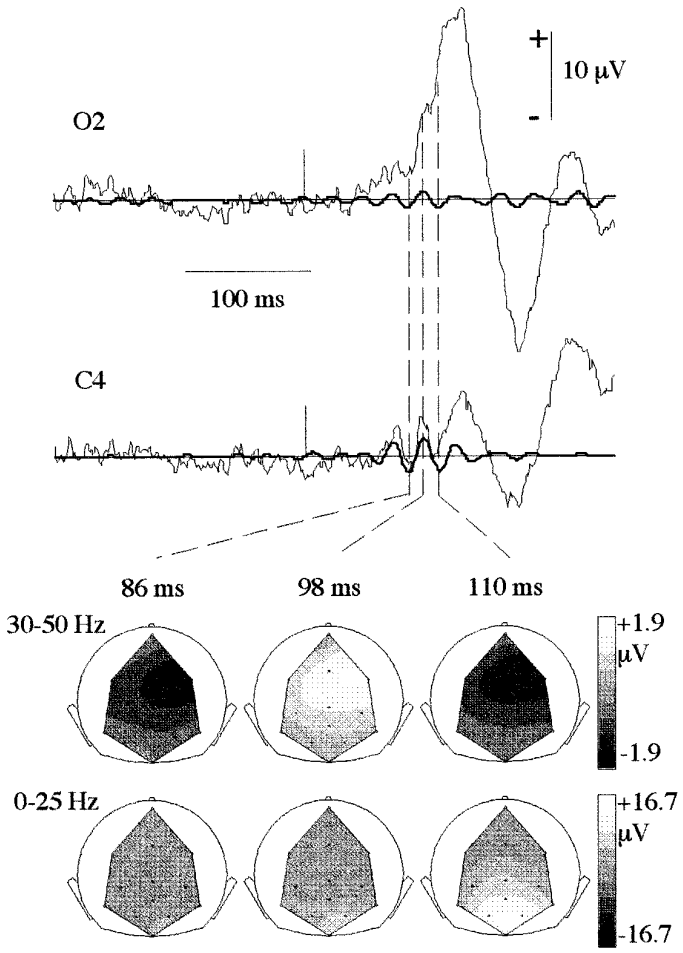

Figure 9. Comparison of the first 40 Hz component to the low-frequency P1 of the evoked response. The broad-band averaged evoked potential (*thin line*) of a typical subject is presented at two electrodes, superimposed with the 30–50 Hz filtered evoked potential (*thick lines*). The *vertical bar* indicates stimulus onset. The oscillatory 40 Hz event occurs at *C4*, whereas the low-frequency P1 is rising at *O2*. Note the amplitude difference between the two events. The topographies of the 30–50 Hz and 0–25 filtered evoked potential are shown at three latencies: they are clearly distinct.

ponent is part of a broad-band response, because the low-frequency components behave differently and have different topographies. A similar gamma-band response, not phase-locked to stimulus onset and occurring between 200 and 400 msec, has been observed in the auditory modality, in the EEG of fast-reacting subjects (Jokeit and Makeig, 1994), and in the epipial EEG of rat (Franowicz and Barth, 1995).

We do not know in which structures this scalp-recorded 40 Hz activity originates. Possible loci for such high-frequency synchronized activity are the hippocampus (Leung, 1992; Bragin et al., 1995), the cingulate cortex (Leung and Borst, 1987), and of course the visual system. The widespread topography and high amplitude of the scalp-recorded 40 Hz activity suggest that it corresponds either to a rather deep and strong activity or to an activity widely distributed across many cortical (or subcortical) areas. In either case, it must be very well synchronized to be recorded with such an amplitude on the scalp. Both of these interpretations are supported by the study of Hirsch et al. (1995) in human using fMRI, which (1) suggests the existence of a "common locus of processing for the contour, whether real or perceptually generated," located below the calcarine sulcus, probably in area 18, and (2) shows that the activity associated with the perception of illusory contours "occur in multiple foci."

Because the origin of the scalp-recorded activity we observe is not known, it is difficult to compare it directly with local field potentials or multi-unit activities recorded from a few neurons within one or two areas in the animal. Nevertheless, the 40 Hz activity we observe shows some similarities with the oscillatory events elicited by a visual stimulus recorded in the animal:

- the scalp-recorded activity is not phase-locked to the stimulus onset, like the oscillatory events recorded in cat (Eckhorn et al., 1988; Gray and Singer, 1989; Gray et al., 1989, 1990, 1992; Brosch et al., 1995) and in monkey (Eckhorn et al., 1993).
- the activity we describe lasts between ~100 and ~150 msec. Oscillations in local field potentials have been estimated to last from 100 to 200 msec in the anesthetized cat (Gray et al., 1992), and from 100 to 300 msec in the superior temporal sulcus of the awake monkey (Kreiter and Singer, 1992). Irregular bursts in the 20–40 Hz of the monkey EEG last between 75 and 200 msec (Freeman and van Dijk, 1987).
- both the activity we describe and the high-frequency synchronization observed by Gray et al. (1989) and Engel et al. (1991) are stronger in response to coherent stimuli.

All of these comparisons are made with experiments on animal using moving stimuli, whereas those we used in our study were stationary. Stationary stimuli have been shown to elicit few or no oscillatory events in cat (Gray et al., 1990) and monkey (Tovee and Rolls, 1992; Young et al., 1992). Nevertheless, Gray et al. (1995) reported recently that stationary stimuli actually elicit oscillatory events in the awake monkey.

Low-frequency evoked potential components display an increased negativity in response to the illusory triangle between 200 and 300 msec, as already found by Sugawara and Morotomi (1991). The effect we observe in low-frequency potentials is distinct from the effect found in the 40 Hz range, indicating that high- and low-frequency components of the response have different functional roles. Still, the precise role of this low-frequency component (0–8 Hz) remains unclear, as well as its origin. Neurons in V2 (von der Heydt et al., 1984) as well as in V1 (Grosof et al., 1993) have been shown to respond to illusory contours, but we have no evidence yet that the low-frequency negativity associated with processing of illusory contours we observe originates in V1/V2.

Probably both low- and high-frequency synchronizations participate in the processing of the illusory and real triangles, but in different manners. The functional links between these two types of activities remain to be explored, and functional models integrating low- and high-frequency activities devised.

REFERENCES

Bertrand B, Pantev C (1994) Stimulus frequency dependence of the transient oscillatory auditory evoked responses (40 Hz) studied by electric and magnetic recordings in human. In: Oscillatory event-related brain dynamics (Pantev C, Elbert T, Lütkenhöner B, eds), pp 135–146. New York: Plenum.

Bragin A, Jandó G, Nádasky Z, Hetke J, Wise K, Buzsáki G (1995) Gamma (40–100 Hz) oscillation in the hippocampus of the behaving rat. J Neurosci 15:47–60.

Brosch M, Bauer R, Eckhorn R (1995) Synchronous high-frequency oscillations in cat area 18. Eur J Neurosci 7:86–95.

Chatrian GE, Bickford RG, Uihlein A (1960) Depth electrographic study of a fast rhythm evoked from the human calcarin region by steady illumination. Elec Clin Neurophysiol 12:167–176.

Conover WJ (1980) Practical nonparametric statistics, 2nd Ed. New York, Wiley.

Echallier JF, Perrin F, Pernier P (1992) Computer assisted placement of electrodes on the human head. Elec Clin Neurophysiol 82:160–163.

Eckhorn R (1994) Oscillatory and non-oscillatory synchronizations on the visual cortex and their possible roles in associations of visual features. In: Progress in brain research, Vol 102 (van Pelt J, Corner MA, Uylings HBM, Lopes da Silva FH, eds), pp 405–425. New York, Elsevier.

Eckhorn R, Bauer R, Jordan W, Brosch M, Kruse W, Reitboeck HJ (1988) Coherent oscillations: a mechanism of feature linking in the visual cortex? Biol Cybern 60:121–130.

Eckhorn R, Frien A, Bauer R, Woelbern T, Kehr H (1993) High frequency (60–90 Hz) oscillations in primary visual cortex of awake monkey. NeuroReport 4:243–246.

Engel AK, König P, Singer W (1991) Direct physiological evidence for scene segmentation by temporal coding. Proc Natl Acad Sci USA 88:9136–9140.

Engel AK, König P, Kreiter AK, Schillen TB, Singer W (1992) Temporal coding in the visual cortex: new vistas on integration in the nervous system. Trends Neurosci 15:218–226.

Franowicz MN, Barth DS (1995) Comparison of evoked potentials and high-frequency (gamma-band) oscillating potentials in rat auditory cortex. J Neurophysiol 74:96–112.

Freeman WJ, van Dijk BW (1987) Spatial patterns of visual cortical fast EEG during conditioned reflex in a rhesus monkey. Brain Res 422:267–276.

Frien A, Eckhorn R, Bauer R, Woelbern T, Kehr H (1994) Stimulus-specific fast oscillations at zero phase between visual areas V1 and V2 of awake monkey. NeuroReport 5:2273–2277.

Galambos R, Makeig S, Talmachoff PJ (1981) A 40-Hz auditory potential recorded from the human scalp. Proc Natl Acad Sci USA 78:2643–2647.

Ghose GM, Freeman RD (1992) Oscillatory discharge in the visual system: does it have a functional role? J Neurophysiol 68:1558–1574.

Gray CM, Singer W (1989) Stimulus-specific neuronal oscillations in orientation columns of cat visual cortex. Proc Natl Acad Sci USA 86:1698–1702.

Gray CM, König P, Engel AK, Singer W (1989) Oscillatory responses in cat visual cortex exhibit inter-columnar synchronization which reflects global stimulus properties. Nature 338:334–337.

Gray CM, Engel AK, König P, Singer W (1990) Stimulus-dependent neuronal oscillations in cat visual cortex: receptive fields properties and feature dependence. Eur J Neurosci 2:607–619.

Gray CM, Engel AK, König P, Singer W (1992) Synchronization of oscillatory neuronal responses in cat striate cortex: temporal properties. Vis Neurosci 8:337–347.

Gray CM, Friedman-Hill SR, Maldonado PE (1995) Stimulus-dependent neuronal oscillations in areas V1 and V2 of the alert macaque monkey. Soc Neurosci Abstr 592:2.

Grosof DH, Shapley RM, Hawken MJ (1993) Macaque V1 neurons can signal "illusory" contours. Nature 365:550–552.

Grossmann A, Kronland-Martinet R, Morlet J (1989) Reading and understanding continuous wavelets transforms. In: Wavelets, time-frequency methods and phase space (Combes JM, Grossmann A, Tchamitchian P, eds), pp 2–20. New York, Springer.

Hirsch J, DeLaPaz RL, Relkin NR, Victor J, Kim K, Li T, Borden P, Rubin N, Shapley R (1995) Illusory contours activate specific regions in human visual cortex: evidence from functional magnetic resonance imaging. Proc Natl Acad Sci USA 92:6469–6473.

Jervis BW, Nichols MJ, Johnson TE, Allen E, Hudson NR (1983) A fundamental investigation of the composition of auditory evoked potentials. IEEE Trans Biomed Eng 30:43–50.

Jokeit H, Makeig S (1994) Different event-related patterns of γ-band power in brain waves of fast- and slow-reacting subjects. Proc Natl Acad Sci USA 91:6339–6343.

Jokeit H, Goertz R, Küchler E, Makeig S (1994) Event-related changes in the 40 Hz electroencephalogram in the auditory and visual reaction time tasks. In: Oscillatory event-related brain dynamics (Pantev C, Elbert T, Lütkenhöner B, eds), pp 135–146. New York: Plenum.

Kanizsa G (1976) Subjective contours. Sci Am 235:48–52.

Kreiter AK, Singer W (1992) Oscillatory neuronal responses in the visual cortex of the awake macaque monkey. Eur J Neurosci 4:369–375.

Kronland-Martinet R, Morlet J, Grossmann A (1987) Analysis of sound patterns through wavelet transforms. Int J Pattern Recognit Artificial Intelligence 1:273–302.

Leung SL (1992) Fast (beta) rhythms in the hippocampus: a review. Hippocampus 2:93–98.

Leung SL, Borst JGG (1987) Electrical activity of the cingulate cortex. I. Generating mechanisms and relations to behavior. Brain Res 407:68–80.

Llinás R, Ribary U (1993) Coherent 40-Hz oscillations characterizes dream state in human. Proc Natl Acad Sci USA 90:2078–2081.

Makeig S (1993) Auditory event-related dynamics of the EEG spectrum and effects of exposure to tones. Elec Clin Neurophysiol 86:283–293.

Maunsell JHR, Gibson JR (1992) Visual responses latencies in striate cortex of the macaque monkey. J Neurophysiol 68:1332–1344.

Milner PM (1974) A model for visual shape recognition. Psychol Rev 81:521–535.

Pantev C, Makeig S, Hoke M, Galambos R, Hampson S, Gallen C (1991) Human auditory evoked gamma-band magnetic fields. Proc Natl Acad Sci USA 88:8996–9000.

Ribary U, Ioannides AA, Singh KD, Hasson R, Bolton JPR, Lado F, Mogilner A, Llinás R (1991) Magnetic tomography of coherent thalamocortical 40-Hz oscillations in humans. Proc Natl Acad Sci USA 88:11037–11041.

Regan D (1968) A high frequency mechanism which underlies visual evoked potentials. Elec Clin Neurophysiol 25:231–237.

Sugawara M, Morotomi T (1991) Visual evoked potentials elicited by subjective contour figures. Scand J Psychol 32:352–357.

Sinkkonen J, Tiitinen H, Näätänen R (1995) Gabor filters: an informative way for analyzing event-related brain activity. J Neurosci Methods 56:99–104.

Tallon C, Bertrand O, Bouchet P, Pernier J (1995) Gamma-range activity evoked by coherent visual stimuli in humans. Eur J Neurosci 7:1285–1291.

Tovee MJ, Rolls ET (1992) Oscillatory activity is not evident in the primate temporal visual cortex. NeuroReport 3:369–372.

von der Heydt R, Peterhans E, Baumgartner G (1984) Illusory contours and cortical neuron responses. Science 224:1260–1262.

Young MP, Tanaka K, Yamane S (1992) On oscillating neuronal responses in the visual cortex of the monkey. J Neurophysiol 67:1464–1474.